Microstructural and Mechanical Investigation on Fiber Laser Welding of S500MC Steel

Mahmoud Moradi[1*], Kianosh Kornokar[2], Fardin Nematzadeh[2*], Hossein Mostaan[2], Saleh Meiabadi[3*], Vincent Demers[3], Jonathan Lawrence[4]

[1]Faculty of Arts, Science and Technology, University of Northampton, Northampton NN1 5PH, UK. Mahmoud.Moradi@northampton.ac.uk
[2]Department of Materials and Metallurgical Engineering, Faculty of Engineering, Arak University, Arak 38156-88349, Iran; kornokarkianosh@gmail.com ; h-mostaan@araku.ac.ir
[3]Department of Mechanical Engineering, École de technologie supérieure, 1100 Notre-Dame West, Montreal, QC, H3C 1K3, Canada. mohammadsaleh.sheikhmohammadmeiabadi.1@ens.etsmtl.ca; vincent.demers@etsmtl.ca
[4]School of Computing, Engineering & Physical Sciences, University of the West of Scotland (UWS), High Street, Paisley PA1 2BE, UK. jl-laserengineering@hotmail.com
*****Correspondence: Mahmoud.Moradi@northampton.ac.uk; f-nematzadeh@araku.ac.ir ; mohammadsaleh.sheikhmohammadmeiabadi.1@ens.etsmtl.ca

Abstract
In recent decades, laser beam welding of high strength low alloy steel has replaced some other assembly processes used in automotive, machinery, and agricultural equipment sectors. In this research, the effect of heat input on the microstructure and mechanical properties of the butt joint of high strength low alloy steel S500MC, which had strengthened by thermomechanically controlled processing, was investigated. The joining process was performed in an autogenous mode at two different heat inputs (140 and 240 J/mm) using the laser beam welding process with a fiber source. Microstructural observations with an optical microscope and scanning electron microscope indicate that the microstructure of the fusion zone consists of acicular ferrite and scattered martensite packets. An increase of heat input reduced the contribution of martensite packets in the fusion zone. The presence of carbides in the coarse grained heat affected zone created fine martensitic packet moreover the packet size has increased with the higher heat input and the dissolution of carbides. In addition to the microstructural changes, the grain size in the weld zone and heat affected zone becomes larger than those observed in the base metal consequently, the properties resulting from the controlled thermomechanical treatment have been lost in both zone. This autogenous welding process produced a decrease in hardness in the fusion zone but an increase in local strength in the heat affected zone compared to the unaffected base metal. Tensile test confirmed that the fracture occurred within the mechanically weaker fusion zone. But at a high input of 240 J/mm due to the decrease volume fraction of martensite and coarse grain size, the strength of the fusion zone reaches 581 MPa, which shows a decrease of about 10% compared to the 140 J/mm heat input.

Keywords
S500MC steel; Laser beam welding; Heat input; Microstructure.

1. Introduction
In recent years, laser welding has expanded greatly due to its inherent advantages over other welding methods in various industries, especially automotive, shipbuilding, aerospace, and microelectronics. The most important advantages of laser welding are accuracy, higher speed, low heat input, reduced thermal stress, successful welding of heat-sensitive parts, high automation capability, and high potential for welding of dis-similar metals [1, 2]. This industrial welding

process has great interest towards more controllability and fewer preparation steps which are the potential features of laser welding [3-5]. S500MC steel is a high strength low alloy steel (HSLA) which is manufactured ac-cording to DIN EN10149-2 standard. S500MC steel is originally designed for marine and offshore structures [6] and manufactured through thermomechanical controlled process (TMCP) with controlled heating and cooling cycles to maximize strength and toughness. The optimal mechanical properties in TMCP steels are attained due a superior control over the rolling steps at a certain temperature that produce an exceptionally fine-grained microstructure [7]. A combination of strength, toughness, and excellent ductility has caused this steel to be used in car body panels and chassis, agricultural machinery, and bridges [8-11]. Despite poor weldability of HSLA steels for underwater welding, S500MC has also applications in ocean technical structures (e.g. oil rigs and pipelines) [12]. In this specific alloy, vanadium and titanium elements form carbide and nitride particles acting as grain growth inhibitors which prevent grain growth process during hot forming, ultimately resulting in both an increase in strength and toughness [13,14].

In addition to these superior mechanical properties, the high weldability of the S500MC steel tend to improve the production rate and reduce production costs. Effects of process parameters used in Gas Metal Arc Welding (GMAW) on the microstructure, mechanical properties, and defects were studied for several S500MC plates [15]. Microstructural analysis exhibited very fine equiaxed grains in the fusion zone (FZ), coarse grained at the FZ/HAZ boundary, and partially refine grained zone on the middle of HAZ. In addition to this heterogeneous microstructure, it was shown that very large grains located around welding porosities was identified as the root cause for the lowest toughness and ductility in the joint. Other works studied the evolution of microstructure and mechanical proper-ties in the fusion zone for dual-phase (DP) steel, HSLA steel, and dissimilar combination of these two alloys joined by fiber laser welding [16]. Transmission electron microscopy (TEM) investigation revealed bainite microstructure in the dissimilar fusion zone comprised of bainitic ferrite embedded with both intra-lath and inter-lath cementite precipitates. Results indicated dispersion of multiple carbides precipitate within the bainitic ferrite laths has a constructive effect on ductile deformation and fracture behavior of dissimilar joints. Using Nd:YAG continuous wave heat source, SA516 grade 70 steel laser welded joints were investigated in order to reveal effects of heat input on microstructure and shape of the weld zone. It was concluded that higher heat input and rapid cooling rate lead to major martensite transformation in the fusion zone. In addition, it was shown that bead width and penetration depth increased with higher heat input [17]. Another study was dedicated to numerically and experimentally investigate solidification cracking during laser welding of advanced high strength steels [18]. Results confirmed that laser welding of high phosphorus Transformation Induced Plasticity (TRIP) steel creates significant segregation of phosphorus at the grain boundaries. The effects of welding input heat on the microstructure and tensile strength of gas tungsten arc welding (GTAW) joints of S500MC steel were investigated. Six heat input levels from low to high were compared in terms of their effects on the evolution of the microstructure in the FZ or in the HAZ and on mechanical properties of the joints. The results showed that the microstructure of the base metal includes ferrite and perlite morphology in an equilibrium state. However, the microstructure of the weld metal most likely changed to lath martensite and retained austenite [19]. Laser welding process was employed for joining HSLA steel plates using Nd:YAG heat source to carry out microstructural investigation on FZ and HAZ. Empirical tests depicted that heat input and cooling rate play significant role in phase transformation so that a decrease in prior austenite grains size was observed at lower heat input [20]. Fiber laser was used to join HSLA plates in order to investigate the effects of heat in-put on the mechanical and microstructural properties of the welding areas. Results concluded that high heat input promotes formation of acicular ferrite, Widmanstätten ferrite, and grain boundary ferrite, while low heat input assists the formation of martensite and bainite. Weld beads containing acicular

ferrite, Widmanstätten ferrite, and grain boundary ferrite demonstrated ductile fracture characteristic with high ductility [21]. An investigation was performed to study microstructure and shape of the fusion zone in laser welding of HSLA using Nd:YAG heat source at different laser speed. Microstructural analysis revealed different ferrites such as needle ferrite, Widmanstätten ferrite, and grain boundary ferrite in the fusion zone. The interesting point was the difference in microstructural phases over weld line so that advancement of the heat source helped the formation of acicular ferrite [22].

Most of the research in this field has been devoted to Nd:YAG laser welding of S500MC steel while the unique feature of fiber laser welding is the focusability and a wide range of beam quality, which can be well suited for autogenous welding. Since the unique mechanical properties of these steels are obtained from the small average grain size caused by the nitrides and carbides, there is a concern that during the welding process, the high heat input causes the dissolution of carbides and nitrides in the HAZ region and creates coarser grains resulting lower toughness and higher hardness [23]. Investigating the effect of heat input on microstructure and mechanical properties of S500MC steel using a fiber laser heat source has received, to the best author's knowledge, only limited attention. Therefore, this work aims to study the influence of fiber laser welding heat input on the evolution of microstructure and the final mechanical performances of S500MC steel joints.

2. Materials and Methods

Joining samples were prepared with dimensions of 1.5 x 30 x 60 mm from S500MC and a quantitative test was performed to determine the chemical composition of the base metal. The results of the quantometric test are presented in Table 1, which corresponded to the chemical composition of S500MC steel. The mechanical properties of this grade of steel according to the UNA-EN-10025 standard are presented in Table 2 as well.

C	Cr	Cu	Mn	Mo	Ni	Si	P	S	Ti
0.10536	0.02923	0.01646	1.64458	0.02167	0.00760	0.13390	0.00982	0.00199	0.00387
N	Sn	V	Al	Pb	B	Nb	Co	W	Fe
0.26031	0.00350	0.00412	0.05491	0.01703	0.00033	0.05867	0.00451	0.01954	97.5962

Table 1. Quantometric chemical test results of S500MC based on weight percentage of elements (wt. %)

Table 2. Mechanical properties of S500MC steel

Strength (MPa)		Elongation	impact energy
Yield	Ultimate	(٪)	(j)
689	776	14 ≤	≤40

Before welding, the plate were ground and clean using acetone to remove the surface oxides and improve the surface quality of the samples that were clamped in the butt joint configuration with no gap. The autogenous welding operation was done in one pass using a fiber laser with a maximum power of 1 kW in a continuous mode using a wavelength of 1064 nm and frequency of 10 Hz. Oxygen was used as the assist gas in the experiments with flow rate of 12 L/min, while a coaxial argon gas shield was used to protect the molten pool. The distance between the nozzle and the surface of the workpiece was set at constant value of 12 mm for all tests so that the focal plane position was kept at the middle of the thickness of the samples which is 0.75 mm below the surface. In order to evaluate the microstructure of the cross-sectional surface of the samples, they were sanded by 2500 grit dry wet sandpaper sheet and then the final polishing was done using diamond paste with 1-micron mesh until an enamel-like finish was achieved. Nital 2% solution was used to

etch samples of S500MC steel. The etching operation was done by immersion method for 5 seconds, then the samples were examined and analyzed by an optical microscope.
The transverse tensile test was used to determine the tensile properties of the samples. Thus, the welded samples were firstly cut according to the ASTM-E8 standard of samples in the direction perpendicular to the welding direction using a wire-EDM and subjected to a tensile test with a Kopa machine. It should be noted that the cross-head speed in the tension test was 2 mm/min. The hardness test was also used to measure the hardness at different points of the welded samples. The test was performed according to the ASTM-E18 standard with a force of 100 kg and a force application time of 15 seconds at ambient temperature. Table 3 shows the fiber laser process parameters for six samples under joining operation that were defined based on preliminary experiments. To investigate the effect of different heat inputs on the microstructure and mechanical properties, the amount of heat input was calculated using equation (1).

$$Q_{laser} = 60*P/S \quad (1)$$

In this equation, Q is the input heat in J/mm, P is the laser beam power (W), and S is the welding speed (mm/min) [24].

Table 3. Fiber laser welding process parameters

Input parameters				Output parameters			
Sample No	Laser Power (W)	Focal plane position (mm)	Welding speed (mm/min)	Heat input (j/mm)	Yield strength (MPa)	Ultimate strength (MPa)	Penetration depth (٪)
1	270	-0.75	75	216	51	116	15
2	270	-0.75	100	162	127	181	20
3	300	-0.75	150	120	227	555	70
4	300	-0.75	200	90	194	576	80
5	350	-0.75	150	140	325	649	100
6	300	-0.75	75	240	291	581	100

3. Results and Discussion

3.1. Effect of Welding Parameters on Weld Pool

Since the samples #1-4 did not reach the full penetration depth, the analysis was focused on samples 5 & 6 that represent two distinctive heat input conditions. As it can be deduced from Table 3 with the increase of the laser beam power and also the increase of the welding speed, the penetration depth is relatively increased and the welding pool goes from the conductive state to the keyhole state, and as a result, the penetration depth is increased. Figure 1 shows the cross-sectional surface of samples #5
and 6 where the full penetration condition can be clearly seen. It can be seen that with the increase of the heat input from 140 to 240 J/mm, significant changes in the shape of the weld pool have taken place, as a result of which the width of the weld has increased from 1.3 mm to 1.8 mm.

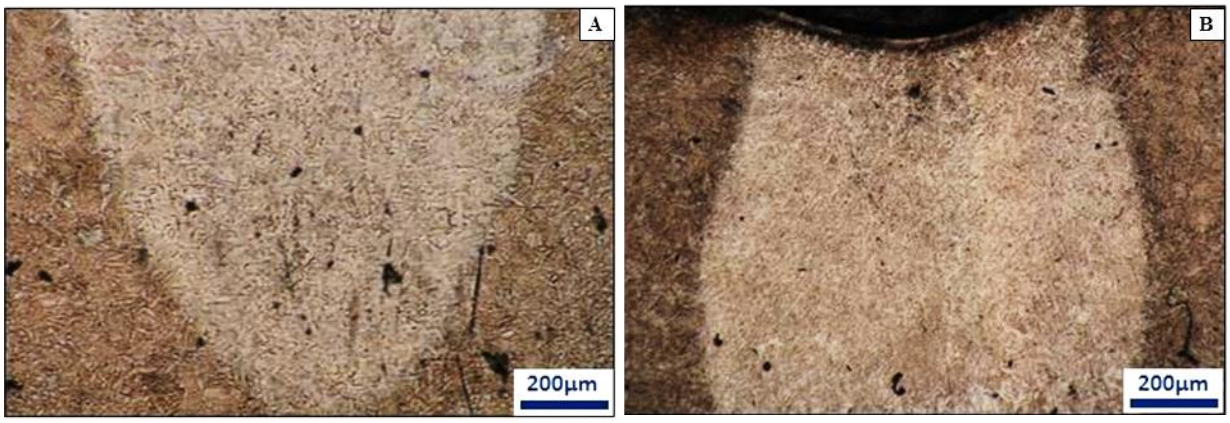

Figure 1. Images of the cross-section of the joint in A) sample #5 (low heat input), and B) sample #6 (high heat input)

3.2. Investigating the Microstructure of Laser Joints

The microstructure of the base metal is shown in Figure 2A. As mentioned above, this steel was produced by thermomechanically controlled processing (TMCP) and was delivered in its normalized state. In this respect, its microstructure consists of ferrite (light phase) and pearlite (dark phase) with very fine ferrite grains. By performing the microhardness test, the average hardness obtained from the cross-section of the base metal is about 220 Vickers. Figure 2B-C presents the microstructure of the fusion zone of both samples showing the dominant microstructure in the welding zone of both samples includes Widmanstätten acicular ferrite and also acicular martensite locally formed in some places. By increasing the heat input and decreasing the cooling rate, the amount of martensite blocks decreased and the contribution of Widmanstätten acicular ferrite increased. Due to the melting process and dissolution of manganese carbides of micro-alloy elements and the loss of the effect of TMCP in the weld zone, the size of the ferrite grains and the dimensions of the packets have become much larger than those observed in the base metal, which has been able to affect the metallurgical and mechanical properties of the joint. Due to the low heat input and high cooling rate during laser welding, hard structures such as bainite or martensite are usually expected to form. However, in the current research, the main microstructure formed in the melting zone was Widmanstätten acicular ferrite. It should be noted that similar microstructures were observed with the samples #1-4. For the formation of hard microstructures, In addition to the cooling rate, the carbon content and distribution are among the most important parameters affecting the formation of hard phases for this HSLA steel. On the other hand, due to the use of a laser fiber heat source and the absence of forces that cause mixing phenomena, such as plasma jets, the weld joint was formed without mixing of elements during solidification. Reasonably formed at the same cooling rate, martensite was locally formed within carbon-rich areas, while Widmannstatten acicular ferrite was formed in the lower carbon content areas.

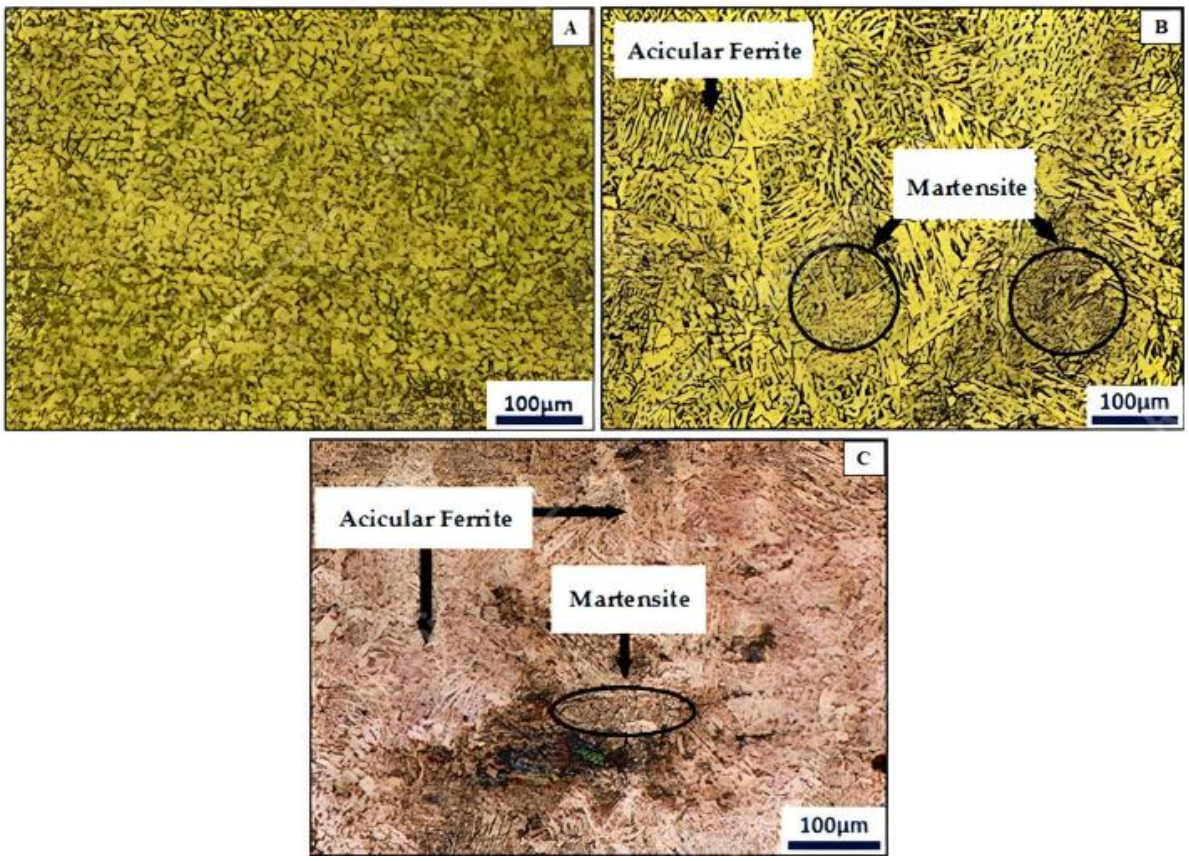

Figure 2. Microstructure of the A) base metal, B) fusion zone in sample #5, and C) fusion zone in sample #6

Figure 3 presents the microstructures formed coarse-grained heat-affected zone (CG-HAZ). Acicular martensite packets were formed due to high temperature experienced by the material in the vicinity of the FZ (i.e., above the eutectoid transformation temperature in the weld) and continued rapid cooling. In this area, due to the dissolution of the carbides of the micro-alloy elements, the grains have been significantly growth compared to the base metal. There is a direct relationship between coarsening of the grains and the increase in input heat so that increasing the heat input has led to the dissolution of most of the carbides in CG-HAZ, and as a result, by removing most of the grain growth barriers, the primary austenite grain size has increased, and finally, the size of the martensite packets has increased with the increase in input heat.

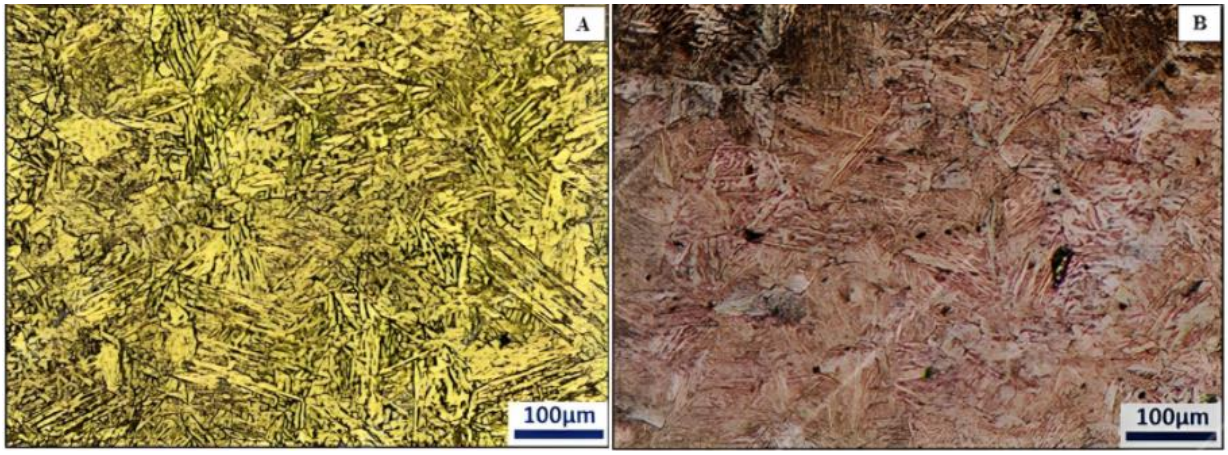

Figure 3. The microstructure of the coarse-structured HAZ in A) sample #5 B) sample #6

The interface between the base metal and the fine grain heat-affected zone (FG-HAZ) is shown in Figure 4. In this specific area the microstructure consists of a soft phase of ferrite with hard islands of martensite, which is characteristic of dual-phase steels (DP). During the welding process in the temperature ranging from 723 to 911°C, the ferrite and austenite phases stable in this high temperature range were transformed in two-phase micro-structure during cooling where ferrite remained unchanged, while the austenite was transformed in martensite. A comparison of Figure 4A-B confirms that an increase of the heat input produced more martensitic phase probably because a higher volume fraction of austenite was formed in this zone when higher heat input and thus temperature is reached.

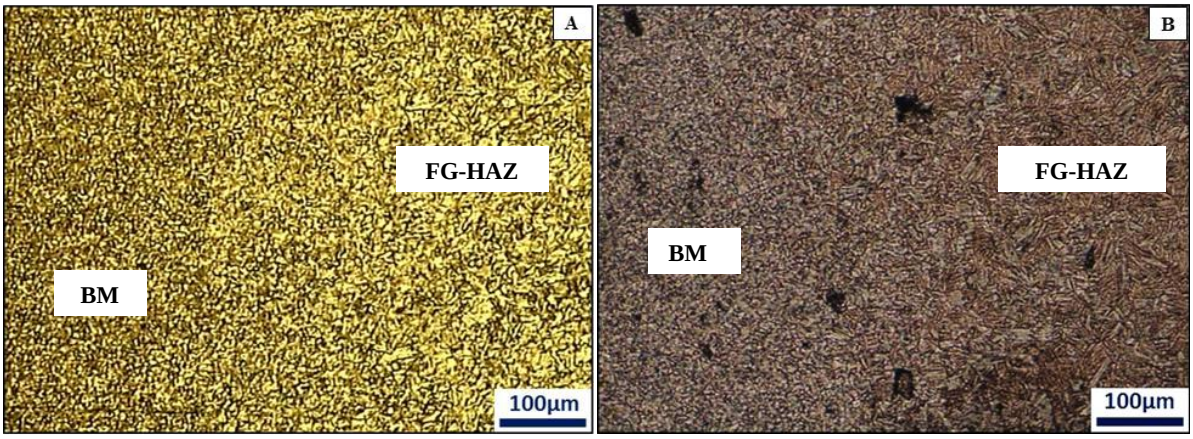

Figure 4. The interface between the base metal and the fine-structure HAZ in A) sample #5 B) sample #6

Extensive changes and transformations occurred in the FZ, CG-HAZ, and FG-HAZ during the welding process. For deeper analysis, high magnification SEM observations of the sample #6 (high heat input) were conducted and are presented in Figure 5. In general, fusion welding, even using an advanced process with low heat input like a laser heat source, ruins the effect of controlled thermomechanical processing. In all zones affected by the heat generated by the fiber laser, grain growth has occurred. It should be noted that the presence of alloy elements in the composition of this steel has created a suitable hardenability causing microstructural changes and developments in addition to the grain growth. Therefore, the microstructure of fusion zone is greatly influenced by the chemical composition of S500MC steel and the heat input of the process and higher heat input leads to slower cooling rate which results in the coarse grains in weld metal. As observed by Kornokar et al [19] on GTAW of the same HSLA steel, similar trend occurred where more martensite as the heat input increases was seen. The results indicated that by the heat input, about

10 times higher than of the current research more martensite microstructure was formed in CG-HAZ, and with the increase of heat input only the size of the packets increased, which shows the role of hardenability in S500MC steel.

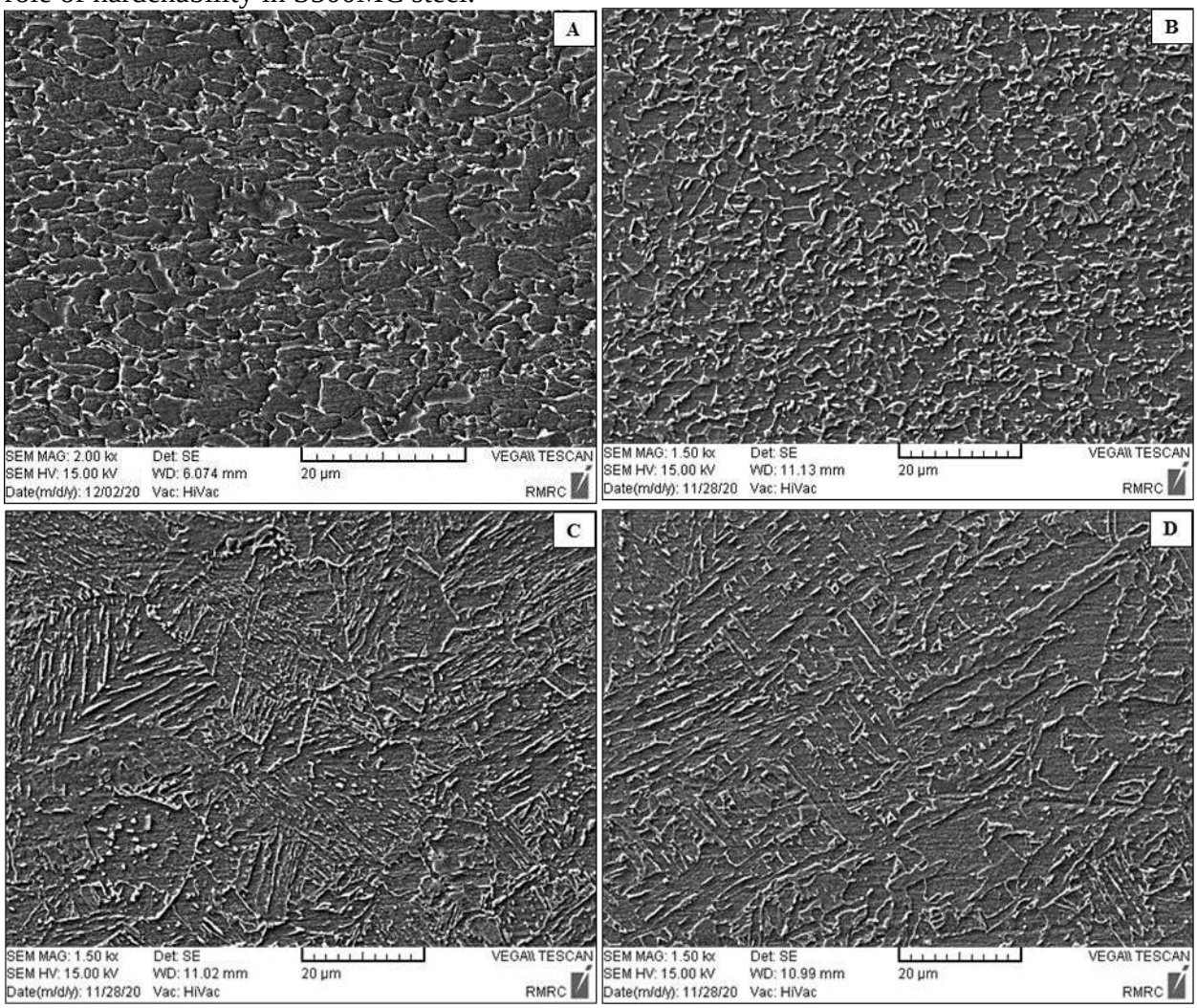

Figure 5. SEM images of the sample #5 with an input heat of 140 J/mm from the areas A) base metal, B) FG-HAZ, C) CG-HAZ, d) FZ

3.3. Examination of Hardness Profile

The hardness profile obtained from the Vickers hardness test along the cross-section of the two welding samples can be seen in Figure 6. The results show that the FZ has the lowest hardness. In this region, the sample #6 exhibits a hardness slightly lower than the sample #5. This is explained by the increase in the heat input from 140 to 240 J/mm forming a microstructure characterized by larger ferrite grain sizes, the absence of carbides, and martensite islands. Similarly in the HAZ, the lower hardness of the sample #6 is due to the increase of heat input that promote dissolution of micro-alloy carbides, which leads to more growth of martensite packets and an increase in ferrite grain size. As a result of the fine-grained structure similar for both sample, the hardness values in the base metal are almost the same. Comparison of different zones, it can be concluded that in both samples, the weld metal zone has the lowest hardness, and the heat-affected zone has the highest hardness value, and among them, sample 5, due to the high heat input, has the lowest hardness with an average of 141 Vickers, which shows a 37.7% decrease in hardness compared to the base metal. But the hardness value in the heat-affected zone was on average 250.66 Vickers, which shows a

9.7% increase compared to the base metal. In contrast, sample 6 has the highest hardness with the lowest heat input and 155.3 Vickers hardness, which shows a 31.3% decrease in hardness compared to the base metal. The heat-affected zone with an average hardness of 257.1 Vickers shows a 15.2% increase in hardness compared to the base metal.

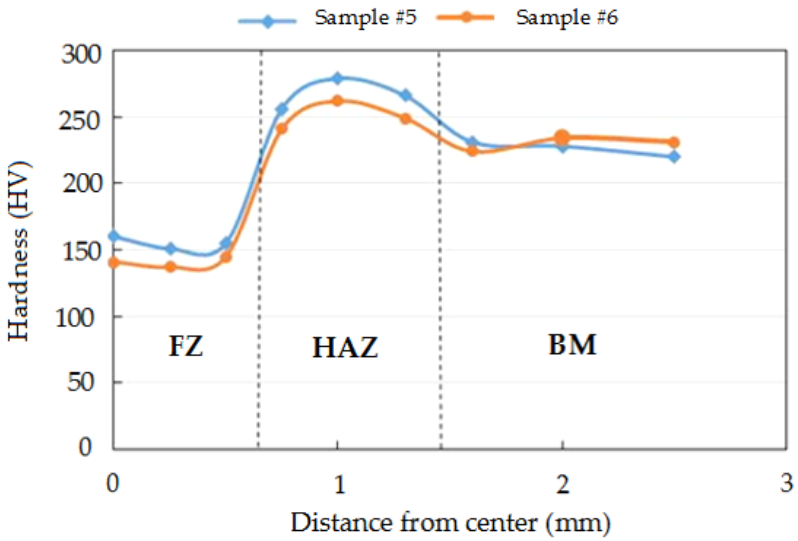

Figure 6. Changes in the hardness profiles of sample #5 and sample #6

3.4. Investigating Mechanical Properties of Joints

Microstructure, grain size, intermetallic compounds as well as external factors such as residual stress, temperature, welding speed, cooling time and type of stress may have an impact on mechanical properties of the joint. Figure 7 shows the dogbone shape samples obtained after the tensile test up to failure displaying all the joint samples failed from the fusion zone. Figure 8 summarized the mechanical properties (YS, UTS, and EL%) obtained from welded sample (#1 to #6) as well as from the base metal (BM). Samples 1-4 did not have a full penetration depth, which resulted in a sharp drop in the tensile properties of the joint. Since these four samples exhibit no full penetration and regardless of the amount of heat input, the ductility of this group (especially for samples #1 and #2) was significantly hindered. The effect of the heat input on the mechanical properties of samples 5 and 6 is investigated.

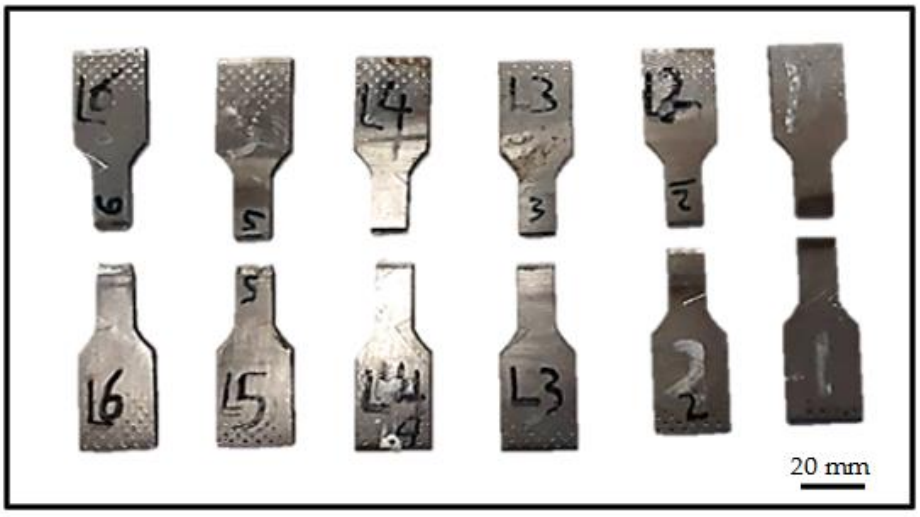

Figure 7. Macroscopic image of tensile samples after failure

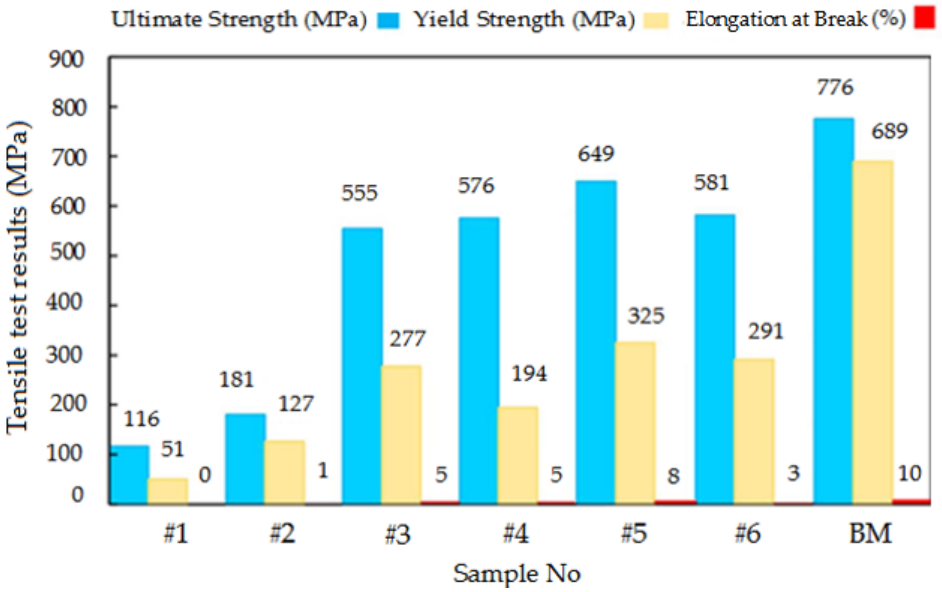

Figure 8. Diagram of the mechanical properties of samples

As can be seen, the lowest tensile strength belongs to sample 6, which has a heat in-put of 240 J/mm. In addition to the high heat input and its effect on the microstructure, it seems that the absence of a welding bead, which is effective in increasing the strength, and the formation of a coarse-grained structure compared to the base metal, resulted in the loss of mechanical properties. The highest tensile strength belongs to sample 5, which has a heat input of 140 J/mm. The strength of the weld metal is lower than that of the base metal and UTS of the sample #5 and #6 is about 84% and 75% of that of the base metal respectively. Since hardness is a measure of local strength, it was observed that the hardness of the FZ is lower than the base metal, and the results of the tensile test also show that the weld metal is less strong than the base metal.

4. Conclusions

The following results were deduced from the research:

- Laser welding of HSLA-S500MC steel without filler ruins the properties resulting from the controlled thermomechanical processing and causes a decrease in the strength of the joining area, resulting in the creation of a weak microstructure, so that the failure of the tensile test samples occurs from the center of the weld.
- Inadequate mixing in the weld pool, non-uniform distribution of alloy elements, and high cooling rate of laser welding at the same time produced a microstructure consisting of Widmanstätten acicular ferrite and locally martensitic islands in the weld metal region.
- As the heat input increased or the cooling rate decreased, the contribution of martensite islands decreased. In the coarse-structured HAZ, acicular martensite was formed, and the size of the packets only increased with the increase of heat input. Also, a two-phase microstructure was formed in the fine- structured HAZ, which increased the contribution of martensite with the increase of heat input. The cause of the aforementioned changes and developments in the loss of TMCP properties, hardness, and the amount of heat input.
- By joining operation, the hardness in the weld metal decreased and increased in the HAZ, and with the increase of the heat input, the greatest decrease in hardness occurred in the weld metal and the greatest increase in hardness occurred in the heat-affected zone. The weld metal shows a 37.7% decrease in hardness, and the heat-affected zone shows a 9.7% increase in hardness compared to the base metal.

- By both heat inputs, the fracture was located in the weld metal, but with low heat input, 16 %, and with high heat input, a 25% decrease in strength compared to the base metal was observed. Therefore, using low input heat, the tensile properties are more favorable and closer to the base metal.

REFERENCES

1. Bagchi, A., Saravanan, S., Kumar, G. S., Murugan, G., & Raghukandan, K. 2017 Numerical simulation and optimization in pulsed Nd: YAG laser welding of Hastelloy C-276 through Taguchi method and artificial neural network. Optik. 146: 80-89.
2. Faraji, A. H., Moradi, M., Goodarzi, M., Colucci, P., & Maletta, C. 2017 An investigation on capability of hybrid Nd: YAG laser-TIG welding technology for AA2198 Al-Li alloy. Optics and Lasers in Engineering. 96: 1-6.
3. Moradi, M., Ghoreishi, M., & Khorram, A. 2018 Process and outcome comparison between laser, tungsten inert gas (TIG) and laser-TIG hybrid welding. Lasers in Engineering (Old City Publishing). 39(3-6): 379-391.
4. Meiabadi, M. S. S. M., Kazerooni, A., Moradi, M., & Torkamany, M. J. 2020 Laser assisted joining of St12 to polycarbonate: Experimental study and numerical simulation. Optik. 208: 164151.
5. Moghanizadeh, A., Honarvar, F., Ghoreishi, M., & Ghajar, R. 2011 An investigation of the parameters affecting the quality of resistance spot welds in low carbon steel sheets. Aerospace Mechanics Journal. 7(2): 1-9.
6. Fydrych D, Łabanowski J, Rogalski G, Haras J, Tomków J, Świerczyńska A, Jakóbczak P, Kostro Ł. 2014 Weldability of S500MC steel in underwater conditions. Advances in Materials Science. 14(2): 37-45.
7. Perka, A. K., John, M., Kuruveri, U. B., & Menezes, P. L. 2022 Advanced high-strength steels for automotive applications: arc and laser welding process, properties, and challenges. Metals. 12(6): 1051.
8. Coelho, R. S., Corpas, M., Moreto, J. A., Jahn, A., Standfuß, J., Kaysser-Pyzalla, A., & Pinto, H. 2013 Induction-assisted laser beam welding of a thermomechanically rolled HSLA S500MC steel: A microstructure and residual stress assessment. Materials Science and Engineering: A. 578: 125-133.
9. Blackman, S. A. 2003 An economic assessment of mechanized welding of high-strength linepipe for the Australian pipeline industry. Pipes & pipelines international (1965). 48(2): 27-37.
10. Ramirez, J. E. 2008 Characterization of high-strength steel weld metals: chemical composition, microstructure, and nonmetallic inclusions. WELDING JOURNAL-NEW YORK. 87(3): 65.
11. Gardiola B, Humbert M, Esling C, Flemming G, Hensger KE. 2001 Determination and prediction of the inherited ferrite texture in a HSLA steel produced by compact strip production. Materials Science and Engineering: A. 303(1-2): 60-69.
12. Fydrych D, Rogalski G, Łabanowski J. 2014 Problems of underwater welding of higher-strength low alloy steels. Institute of Welding Bulletin. 5: 187-195.
13. Verdeja JI, Asensio J, Pero-Sanz JA. 2003 Texture, formability, lamellar tearing and HIC susceptibility of ferritic and low-carbon HSLA steels. Materials characterization. 50(1): 81-86.
14. Misra RD, Nathani H, Hartmann JE, Siciliano F. 2005 Microstructural evolution in a new 770 MPa hot rolled Nb–Ti microalloyed steel. Materials Science and Engineering: A. 394(1-2): 339-352.
15. Frih I, Adragna PA, Montay G. 2015 INFLUENCE OF A WELDING DEFECT ON A HSLA S500MC STEEL PLATE: MICROSTRUCTURE AND RESIDUAL STRESS EVALUATION.

In: Proceedings of the 6th International Conference on Mechanics and Materials in Design, pp. 169-180.
16. Saha DC, Westerbaan D, Nayak SS, Biro E, Gerlich AP, Zhou Y. 2014 Microstructure-properties correlation in fiber laser welding of dual-phase and HSLA steels. Materials Science and Engineering: A. 607: 445-453.
17. Oyyaravelu R, Kuppan P, Arivazhagan N. 2016 Metallurgical and mechanical properties of laser welded high strength low alloy steel. Journal of advanced research. 7(3):463-472.
18. Agarwal G, Kumar A, Richardson IM, Hermans MJ. 2019 Evaluation of solidification cracking susceptibility during laser welding in advanced high strength automotive steels. Materials & Design. 183: 108104.
19. Kornokar K, Nematzadeh F, Mostaan H, Sadeghian A, Moradi M, 2022 Waugh DG, Bodaghi M. Influence of Heat Input on Microstructure and Mechanical Properties of Gas Tungsten Arc Welded HSLA S500MC Steel Joints. Metals. 12(4): 565.
20. Palanivel R, Dinaharan I, Laubscher RF. 2020 Microstructure and mechanical behavior of Nd: YAG laser beam welded high strength low alloy steel joints. Optik. 208: 164050.
21. Ribeiro HV, Baptista CA, Lima MS, Torres MA, Marcomini JB. 2021 Effect of laser welding heat input on fatigue crack growth and CTOD fracture toughness of HSLA steel joints. Journal of Materials Research and Technology. 11:801-810.
22. Ramesh R, Dinaharan I, Ravikumar R, Akinlabi ET. 2020 Microstructural characterization and tensile behavior of Nd: YAG laser beam welded thin high strength low alloy steel sheets. Materials Science and Engineering: A. 780: 139178.
23. Nematzadeh F, Karooni H, Noori AL, Moradi M, Roshanaei A, 2018 Investigation of the effect of inlet heat on microstructural properties of the area affected by arc welding heat with manual electrode of vanadium-alloy steels with niobium F70-A 694, In: International Conference on Material Engineering and Metallurgy, pp. 62-69.
24. Meiabadi MS, Kazerooni A, Moradi M. 2018 Numerical Analysis of Laser-assisted Ti to Polyimide Welding Using a Statistical Approach. International Journal of Laser Science: Fundamental Theory and Analytical Methods. 1(2): 185-205.